

Feedback lock-in: A versatile multi-terminal measurement system for electrical transport devices

Cite as: Rev. Sci. Instrum. 94, 013902 (2023); doi: 10.1063/5.0089194

Submitted: 23 February 2022 • Accepted: 15 December 2022 •

Published Online: 4 January 2023



Arthur W. Barnard,^{1,2,3,a)} Evgeny Mikheev,^{1,4} Joe Finney,¹ Han S. Hiller,² and David Goldhaber-Gordon^{1,4,a)}

AFFILIATIONS

¹ Department of Physics, Stanford University, Stanford, California 94305, USA

² Department of Physics, University of Washington, Seattle, Washington 98195, USA

³ Department of Materials Science and Engineering, University of Washington, Seattle, Washington 98195, USA

⁴ SLAC National Accelerator Laboratory, Menlo Park, California 94025, USA

^{a)}Authors to whom correspondence should be addressed: awbl@uw.edu and golhaber-gordon@stanford.edu

ABSTRACT

We present the design and implementation of a measurement system that enables parallel drive and detection of small currents and voltages at numerous electrical contacts to a multi-terminal electrical device. This system, which we term a feedback lock-in, combines digital control-loop feedback with software-defined lock-in measurements to dynamically source currents and measure small, pre-amplified potentials. The effective input impedance of each current/voltage probe can be set via software, permitting any given contact to behave as an open-circuit voltage lead or as a virtually grounded current source/sink. This enables programmatic switching of measurement configurations and permits measurement of currents at multiple drain contacts without the use of current preamplifiers. Our 32-channel implementation relies on commercially available digital input/output boards, home-built voltage preamplifiers, and custom open-source software. With our feedback lock-in, we demonstrate differential measurement sensitivity comparable to a widely used commercially available lock-in amplifier and perform efficient multi-terminal electrical transport measurements on twisted bilayer graphene and SrTiO₃ quantum point contacts. The feedback lock-in also enables a new style of measurement using multiple current probes, which we demonstrate on a ballistic graphene device.

Published under an exclusive license by AIP Publishing. <https://doi.org/10.1063/5.0089194>

INTRODUCTION

Electrical transport measurements play a central role in understanding the behavior of electrons in solids. Such measurements involve sourcing currents and/or voltages in particular locations on a “device”—a material or set of materials structured in some well-defined geometry—and probing how the resultant voltages and/or currents measured at the same or different locations within the device vary with external control parameters (e.g., temperature, magnetic field, and electric field). When the material is patterned on small length scales—the so-called mesoscopic regime¹—electrical transport measurements can reflect quantum mechanical wave behavior, ballistic motion, Coulomb interactions, and topological properties that are hidden on familiar macroscopic scales. In this

regime, physical phenomena can be highly sensitive to the magnitude of applied currents and voltages. So, to probe such devices it is critical to keep these excitations small, which in turn creates a need to measure small signals. To this end, lock-in amplifiers are commonly used to measure small signals amid comparatively large background noise by measuring a narrow-bandwidth response at the frequency of a sinusoidal drive signal.

Lock-in techniques are effective at filtering out noise; however, there is an inverse relationship between the amount of filtering and the averaging time needed to perform a single measurement.² Thus, transport measurements are inherently speed-limited, and it often takes weeks to months to study a single device, especially if its behavior as a function of multiple parameters is of interest. Given the considerable expense in time and resources to perform such

measurements, it is valuable to parallelize data acquisition. Modern condensed matter physics increasingly relies on multi-terminal devices to probe the physics of new materials;^{3–6} so, the ability to efficiently probe 10 or more channels simultaneously can dramatically accelerate the discovery process and avoid requiring experimentalists to pre-select which subset of data to take.

Commercial and homebuilt multi-channel,^{7–9} low-cost, computer-based^{10–13} lock-in amplifiers have been developed for a variety of applications. Recent developments,^{14–20} based on commercial FPGAs, compare favorably with common commercial lock-in amplifiers. However, to date such approaches have not made a significant impact on studies of mesoscopic devices, in part because a multi-terminal system hasn't been demonstrated in a configuration tailored to quantum transport devices.

Here, we demonstrate such an instrument, which can be built from discrete components and commercially available data acquisition boards, at a total price comparable to that of a single, commercial lock-in amplifier. Besides replacing the function of many lock-in amplifiers inexpensively and compactly, this system's capability to programmatically switch the effective impedance of individual measurement leads enables versatile control over the measurement configuration, including accessing configurations that would otherwise be practically impossible to achieve.

FEEDBACK LOCK-IN DESIGN

Our measurement system, which we term a feedback lock-in, combines commercial digital acquisition boards (from National

Instruments—henceforth NI—in our present design) with home-built voltage amplifier boards and custom open-source software running on a consumer-grade desktop PC. It operates by sourcing sinusoidal currents and measuring the voltage response for each period of the sine wave. The in-phase (V_x) and out-of-phase (V_y) components are computed and can be averaged or fed back on to adaptively change the source current amplitude. When no feedback is used, the source impedance is naturally high; however, when feedback is on, a source can act as a low-impedance virtual ground. This low-impedance exists in a narrow frequency band around the drive frequency, retaining a high-impedance at other frequencies, which prevents voltage noise sources and voltage offsets from driving significant currents through a device.

The basic configuration for a single channel measurement is outlined in Figs. 1(a) and 1(b). A software-generated sinusoidal voltage signal passes through a high-impedance bias resistor to an electrical lead of the device. The voltage response of the same (or different) lead is then read in through a variable gain preamplifier, whose output is digitized by a commercial analog-to-digital converter (ADC) channel. The recorded voltages are then multiplied by in-phase and out-of-phase reference sine waves and the results numerically integrated to produce the measured V_x and V_y components. The measured components can then be time-averaged using computer-defined window functions (e.g., exponential or rectangular) to improve the signal-to-noise ratio (SNR). The averaged signal can then be passed to a software-defined digital proportional-integral (PI) loop to enable adaptive control of the source current.

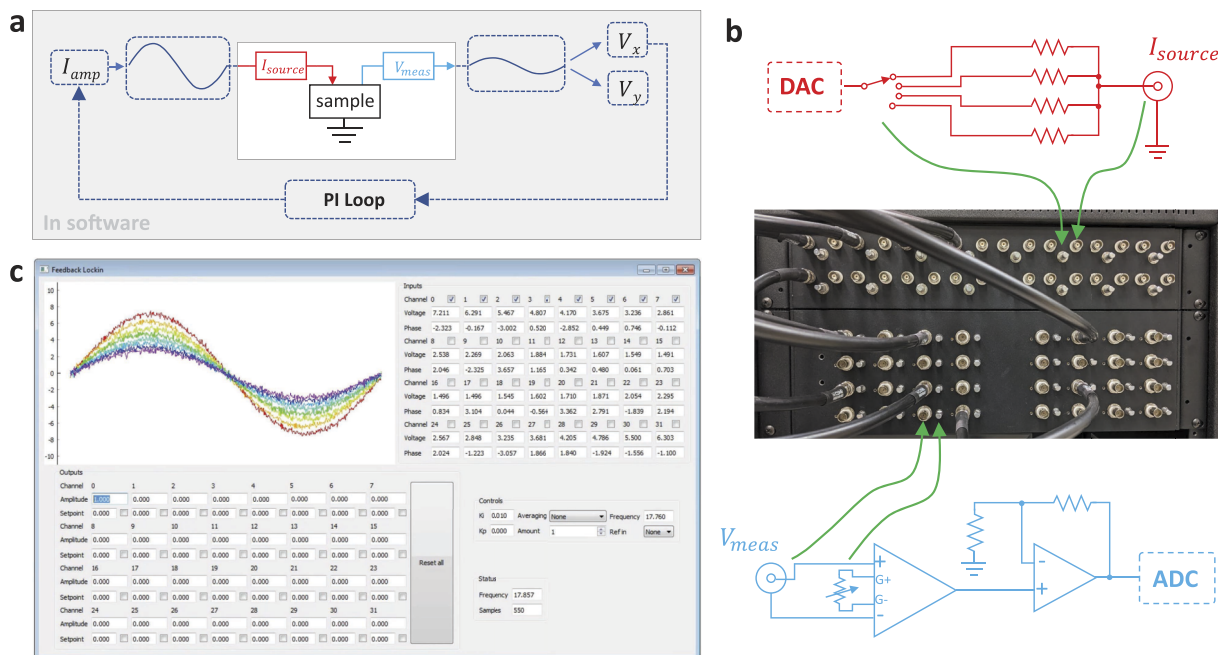


FIG. 1. Feedback lock-in design. (a) Schematic of operation of feedback lock-in for a single channel on a 2 (or 3) terminal device. The computer generates a sinusoidal drive signal that passes through a DAC and a bias resistor to provide current I_{source} to the sample. Voltage V_{meas} is collected, amplified, and read-in to software via an ADC. The result is multiplied by a sine and cosine wave and integrated to produce V_x and V_y . An optional feedback loop can adjust the sourced current to maintain a V_{meas} setpoint. (b) Hardware implementation. Current source is diagrammed in red, and voltage measurement is diagrammed in teal. The 32 outputs each have 3–4 selectable bias resistors, and the 32 inputs have 3–4 selectable gain settings. (c) Graphical user interface.

The proportional gain is typically set at zero, but available to increase feedback stability. In the 2-terminal configuration depicted in Fig. 1(a), the feedback loop can be used to effectively enable a voltage-biased measurement (wherein the source current serves as the dependent variable probed). The single channel behavior can be easily generalized, so that one or more currents are sourced, and a large number of voltages are measured simultaneously. For maximum flexibility, one current source can be provided per input-channel.

Because much of the feedback lock-in operation is carried out in software, there is flexibility to add functionality that is uncommon in stand-alone lock-ins. For example, the sliding window average is particularly effective for transport measurements, since it allows the user to maximize the number of sinusoidal cycles averaged for each data point without a risk of unintended bleedthrough between data points in exponential averaging (low pass filtering).

SOFTWARE INTERFACE

Our open-source homebuilt software interface is written in Python, using the PyVISA driver platform to communicate with NI boards. It includes a simple TCP server, allowing external programs (including those not based on Python) to control and read out the instrument's status. An example of the graphical user interface (using PySide2) is shown in Fig. 1(c). Based on conditions set in a configuration file, the software automatically populates the UI with the appropriate number of input/output channels, enabling designs relying on different NI boards.

In the upper right of Fig. 1(c), the amplitude and phase of each of the 32 channels are displayed. For each channel, a checkbox toggle determines whether a real-time oscilloscope trace is plotted in the upper left. In the lower left, the 32 outputs' amplitudes can be directly set or controlled by a feedback loop setpoint when the associated checkbox is set. In the lower right are global control parameters, including the PI loop constants (K_i and K_p), type of averaging, lock-in frequency, and an option to set a reference input signal for the feedback loops. This reference signal is a user-selectable one of the 32 inputs, which is then subtracted from other inputs to aid in establishing a local ground signal for feedback measurements. Finally, a "Reset all" button in the lower middle gives the user a quick way of aborting a measurement to avoid damage to a device.

IMPLEMENTATION OF FEEDBACK LOCK-IN

Our feedback lock-in approach combines software and hardware with flexibility on specific details of the implementation, which may be tailored to a user's application. In our case, we developed our system to meet the needs of our quantum transport labs, and our demonstrated implementation may be valuable among this research community.

Voltage preamplifiers

The feedback lock-in relies critically on accurate measurements of μV voltages, and, as such, voltage preamplifiers are required. Given that the system has 32 implemented channels, we opted to build a scalable homebuilt preamplifier board (Fig. 2). These boards

are designed with on-board voltage regulators with capacitive/inductive power supply filters, and each has four individual voltage preamplifiers (and, thus, we used 8 boards in our implementation). We supply these boards with a $+/- 15$ V commercial DC supply (Acopian TD15-160) and regulated them down to $+/- 12$ V with standard solid state voltage regulators (LM7912/LM7812). Each channel uses an isolated BNC jack, with the inner and outer conductors routed to the positive and negative inputs of a single-resistor gain-programmable instrumentation amplifier (LT1920), which has low noise characteristics ($7.5 \frac{\text{nV}}{\sqrt{\text{Hz}}}, 124 \frac{\text{fA}}{\sqrt{\text{Hz}}}$, 2.5 Hz 1/f corner frequency). We implement four gains, selectable by a rotary switch, with gains including 10^2 , 10^3 , 10^4 , and 10^5 . For each channel, a voltage offset potentiometer is used, buffered by a unity gain follower on a separate dual op-amp chip (LT1112). Finally, the output of the instrumentation amplifier is buffered, filtered, and amplified with the other side of the dual op-amp chip. We use a $\times 10$ gain and 500 Hz corner frequency on this amplifier based on the signal strength and frequencies with which we typically operate. Given the $\times 10$ additional gain, our final gains are 10^2 , 10^3 , 10^4 , and 10^5 . The amplified output voltages are then directly wired to a commercial analog-to-digital converter (ADC) board (NI PCIe-6363) via a screw terminal block (NI SCB-68A).

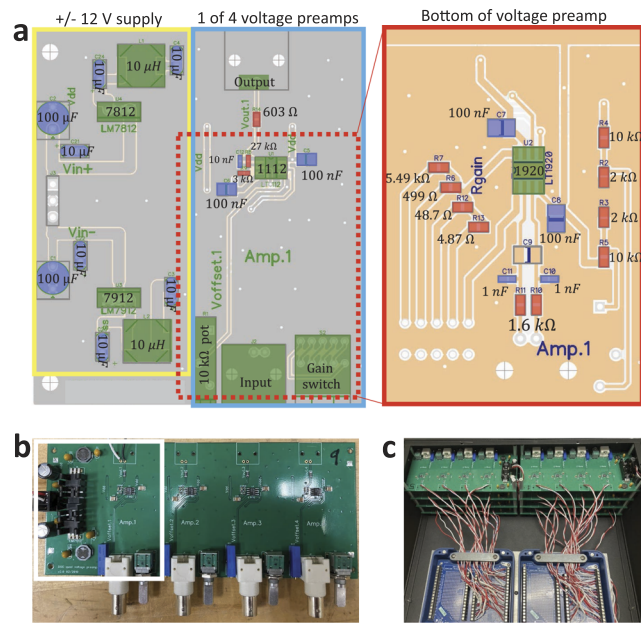


FIG. 2. Voltage preamplifier design. (a) Board layout of a single channel preamplifier, including the board power supply. Capacitors are labeled in blue, resistors in red, and others in green. The power supply (yellow border) uses linear voltage regulators and capacitor/inductor filtering to supply $+/- 12$ V to four identical voltage preamplifiers. The preamplifier uses an LT1920 instrumentation amplifier, with gain set by a rotary switch, and gain resistors. The output is buffered, amplified, and filtered by an LT1112 operation amplifier to yield total gains of 10^2 , 10^3 , 10^4 , and 10^5 . A trimming potentiometer is used to zero-out DC offsets. (b) Fully populated board with four preamplifiers; white box indicates the region shown in (a). (c) 8 boards are housed in a single box with DC supply voltages daisy-chained and signal outputs routed to screw terminal boxes (NI SCB-68A). Signals are read-in by an ADC board (NI PCIe-6363).

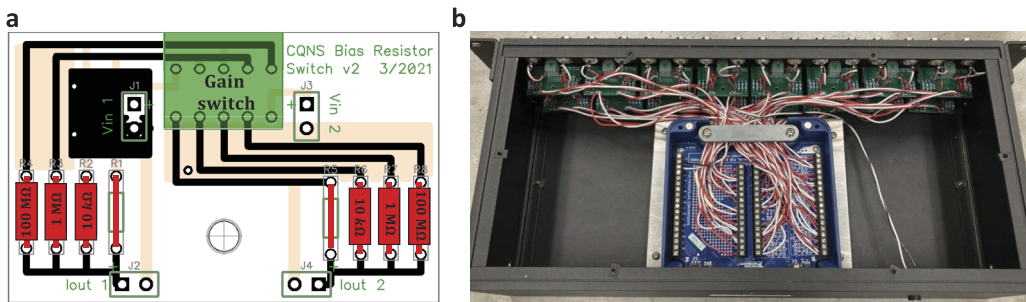


FIG. 3. Output current sources. (a) Board layout for two channels of user-selectable bias resistors that share a 2-pole gain switch. A DAC board (NI PCIe-6738) supplies AC signals up to $10 V_p$ to the V_{in} via a screw terminal box (NI SCB-68A). Bias resistor values include $10 \text{ k}\Omega$, $1 \text{ M}\Omega$, and $100 \text{ M}\Omega$, as well a low impedance line, to allow for external choices of gain resistor. (b) Output box routes to 16 boards, and clock signal (black and white twisted pair) is routed to a jack on the back of the box for synchronizing the output and input clocks.

In the interest of using feedback for a given channel, our implementation is most conveniently configured for single-ended operation, wherein each signal is referenced to the ground. However, it is often desirable to measure samples in a differential configuration, i.e., amplify the difference between voltages at two different terminals on the sample. This is also possible in our voltage preamplifiers, given that each preamplifier amplifies the difference between the inner and outer conductors of a BNC jack. To do so, one must implement external connectors that route two isolated BNC lines to a single amplifier. This can be done individually for a given amplifier (as we did for differential data presented in Fig. 4), or in cases where many differential pairs are desired, one can daisy-chain signals such that a given input serves as a signal for one amplifier and a reference for the next. We built such a box and used it for the data presented in Fig. 5.

Output current sources

Our current sources are made from voltage sources in series with high-impedance bias resistors, as is typical in the quantum transport community. While these outputs are, in principle, not perfect current sources, given that the sample resistance impacts the total current applied, the standard practice in most cases is to use bias resistors with resistances greater than $\times 100$ the sample resistance, limiting the contribution by the sample. Furthermore, one can self-consistently factor in the sample's resistance to recompute the applied current.

To implement our current sources and accommodate measurements of samples spanning a wide range of impedances, we provided three user-selectable bias resistors for each channel—selecting resistors with the lowest available tolerance ratings to ensure uniformity among channels—as well as a low-impedance output for external choices of the bias resistor. We opt for resistors valued at $10 \text{ k}\Omega$, $1 \text{ M}\Omega$ and $100 \text{ M}\Omega$, and use an NI board (PCIe-6738) to supply the output voltages. These outputs can supply $\pm 10 \text{ V}$; so, the peak currents available are 1 mA , $10 \mu\text{A}$, and 100 nA , respectively. The NI board itself is limited to $\pm 10 \text{ mA}$, which will restrict the source only if using the low-impedance output. The amount of current noise injected by these sources is dependent on the voltage noise of the NI board voltage source and the bias resistor. Based

on the board specifications, we estimate our current source to have $\sim 100 \text{ fA}/\sqrt{\text{Hz}}$ as the largest bias resistor setting. This is a similar value to the input-referred noise of our voltage preamplifiers and, thus, does not contribute significantly to the overall measurement noise.

We opted to share one 2-pole gain switch for pairs of outputs to save on front panel real-estate and in acknowledgment of the rarity of needing multiple, different bias resistor magnitudes on each channel [Fig. 3(a)]. As discussed later, this contributes to output channel crosstalk, but at a level that we found small in comparison to typical measurement uncertainties.

Measurement and feedback timing

Our implementation relies on two separate NI boards to enable parallel output and input collection. To synchronize the two boards, we hardwire a clock signal, generated by the output board, followed by the input board. Both boards have internal buffers, which we use to maximize the input/output clock—we write one full sinusoidal cycle to the output buffer and read in one-full sinusoidal cycle from the input buffer. For each cycle, the output is autonomously outputting the buffered signal, while the input is recording voltages to the input buffer. As soon as the input has buffered a full cycle, the data are read to the software, where they are analyzed, and if feedback is in active use, the output amplitude for the next cycle is updated. The delay of one cycle in feedback does not drastically impact the system operation, as we typically need to average over multiple cycles to achieve a suitable signal-to-noise ratio (SNR).

Computing amplitudes for each full cycle simplifies computation. Each full cycle is multiplied by a cosine and sine function and summed to measure the X and Y components without applying discrete filters at the sample clock rate. It also ensures that any recorded data are computed on full cycles, which avoids artifacts, from averaging over fractional cycles. Our subsequent averaging/filtering is then performed on these computed amplitudes with discrete time filters.

Calibration

We calibrate our feedback lock-in using a pre-calibrated Keithley 2450 as a reference standard. For outputs, we determine the

effective bias resistor values by sourcing DC current at positive and negative output voltages at a chosen magnitude and measuring the resultant current from the Keithley 2450. Dividing the difference of the two output voltages and the two resultant currents yields a resistance value insensitive to current or voltage offsets between systems. For inputs, we source current through one of the calibrated current outputs to a grounded resistor whose resistance is determined in advance by the Keithley 2450. Based on the known currents and resistances, we determine the expected voltage measured across the grounded resistor and determine the gain.

In all calibrations, we predetermine a target level of precision and sample sufficient data points whose mean converges to a value within that level of precision. We chose a 1-sigma level of precision to be 10 nV at the highest gain setting, which is crucial, given our choice to carry out measurements that rely on the difference of two single-ended channels rather than only differential measurements. Based on the NI board's absolute accuracy rating (<3 mV at full range), our calibrated outputs should have an accuracy of better than 30 pA when using the 100 MΩ bias resistor.

PERFORMANCE OF FEEDBACK LOCK-IN

To performance-test the feedback lock-in, we measure a surface mount resistor installed on a ceramic chip carrier inside a tabletop vacuum cryostat to ensure that typical noise characteristics are present. We first measure the resistance using a calibrated commercial source-measure unit (model Keithley 2450) in four-wire sense mode. Then, we measure the same resistor using the feedback lock-in, where we use two independent inputs for the high and low voltage terminals in a four-terminal configuration. For the results shown in Fig. 4(a), we use a drive frequency of 17.76 Hz and an exponential averaging with a time constant of 300 ms and sample each configuration once per second for 100 samples. The error bars in Fig. 4(a) correspond to the standard deviation among the single one-second measurements, and, thus, represent the measurement uncertainty, assuming only one one-second sample per experimental configuration. We use source currents (of order 1 nA), which are

at or below typical currents used in transport measurements, and show improved SNR with increasing source current, as expected.

To benchmark the performance of the feedback lock-in, we compare it to a similar measurement performed on a Stanford Research Systems SR830 lock-in amplifier, using an SR560 voltage preamplifier. In Fig. 4(b), we plot the fractional uncertainty as a function of the measured resistance, using three different feedback lock-in configurations and the SR830. The first feedback lock-in configuration (blue circle) is that described above related to Fig. 4(a). The second feedback lock-in configuration (red ×) improves the SNR by routing one sample lead to the center pin and another sample lead to the shield of a single differential voltage amplifier. This is accomplished with a homemade connector that has two isolated BNC inputs routed to a single BNC output. The third configuration also uses a single differential amplifier, but in place of an exponential average, uses a 1 second sliding window. We choose this window size, since we sample data every 1 s. In practice, we average 18 full cycles, which corresponds to 1.01 s.

In measuring with the SR830, we source the current from the feedback lock-in and deliver a reference signal from the feedback lock-in to the SR830 to eliminate variability in output source noise between instruments. We use an SR560 with a newly installed amplifier chip to ensure that there is no additional technical noise introduced by a degraded amplifier. On the SR560, we employ a differential measurement using a $\times 1000$ gain setting, a 0.1 Hz–10 kHz band pass filter, and a low-noise dynamic reserve setting. On the SR830, we maximize the sensitivity (10 mV) and use a 6 dB/dec low pass filter with a 300 ms time constant. Higher order filters are available on the SRS830 (and could be implemented into the feedback lock-in software), though they require shorter time constants to achieve comparable settling times.

The differential measurement condition (red ×) of the feedback lock-in is the most direct comparison to the SR830 + SR560. Both instruments are using low pass filters with similar time constants, and on this metric, the feedback lock-in has comparable performance with ~20% higher uncertainty. However, the feedback lock-in's SNR is improved by utilizing a sliding window average. As

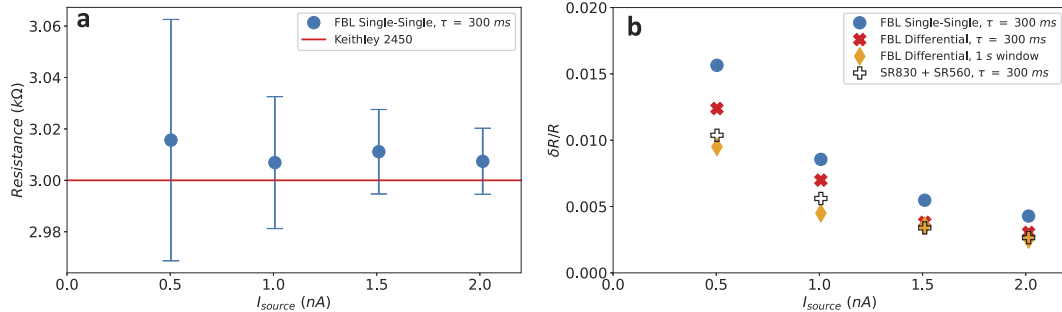


FIG. 4. Performance of feedback lock-in (FBL) in realistic conditions. (a) Measurement of four-terminal resistance of a 3 kΩ resistor inside a tabletop cryostat, measured with frequency 17.76 Hz and a 100 MΩ bias resistor. A reference line for the resistance determined by a calibrated Keithley 2450. The error bars denote the standard deviation δR of 100 successive samples. (b) Measurement modalities compared to those of a commercial lock-in amplifier. The circle data are obtained by measuring terminals on distinct amplifiers and subtracting the measured results. The \times data result from routing the two voltage probes to a differential input of a single amplifier. The diamond data use the same measurement conditions as the \times data, but replace the exponential time average with a windowed time-average. The $+$ denotes the performance of an SR830 lock-in amplifier (6 dB/dec filter setting) and SR560 voltage preamplifier. A single channel of the FBL has noise performance comparable to that of the combined SR830 and SR560.

can be seen, in this condition (orange diamond), the feedback lock-in and SR830 + SR560 have nearly equivalent performances, with the feedback lock-in potentially out-performing the SRS830 + SR560 at low source currents.

As shown, the feedback lock-in's performance is comparable to that of the SR830 for a single channel in realistic transport measurement conditions. It should be noted that the SR830 has high frequency capabilities (102 kHz) that we have not attempted to implement in the feedback lock-in because transport measurements on semiconductors are almost exclusively performed in the 1–100 Hz range to reduce the capacitive/inductive effects of measurement lines. Our implementation multiplexes a 1 MHz sampling clock and consequently has a digital sample rate of 33 kHz per channel—meaning that it is plausible to trade off a reduced number of useable channels to access frequencies comparable to those reached by an SR830. Other RF-based methods speed up measurements, but require specialized expertise and costly external hardware.^{21,22}

As a multichannel instrument, we also characterize the crosstalk. On the output side, we find crosstalk between any two channels is at the most -60 dB at 17.76 Hz. The highest crosstalk specifically arises between pairs of channels that share a common gain switch, and, thus, are routed through a shared printed circuit board. Nearest neighbors not sharing a board have crosstalk of -80 dB level and non-nearest neighbors have crosstalk of <-140 dB. The coupling is likely capacitive and, thus, further isolation strategies beyond twisted pairs should enable all channels to reach this low level of crosstalk. On the input side, we find no evidence of crosstalk (<-80 dB).

EFFICIENTLY PROBING MULTI-TERMINAL DEVICES

As discussed above, if we use the feedback lock-in as a conventional lock-in, its per-channel measurement performance is comparable to that of the SR830 + SR560. However, the feedback lock-in has not just one—but 32 channels. Here, we show this parallelism accelerate measurements in two model multi-terminal devices.

In twisted bilayer graphene, with $\sim 1.1^\circ$ interlayer twist, a moiré superlattice generates a nearly flat sub-band, in which electronic correlations can have dramatic effects.^{23,24} In our and others' work to date, though a specific twist angle between graphene layers is targeted, the actual twist angle commonly varies spatially. In the 22-terminal device shown in Fig. 5(a)²⁵ we simultaneously measure the longitudinal resistance as a function of gate voltage at every pair of neighboring contacts. Note that the carrier density associated with the sub-band filling yields the twist angle in each location, revealing the spatial inhomogeneity of twist angles [Fig. 5(b)]. Also, sweeping magnetic field while still simultaneously acquiring data from each contact pair provides important insights into how twist angle impacts the observed physics.²⁵

Another example of the capability to simultaneously measure many voltage terminals is of nanopatterned 2D electron gases (2DEGs) in SrTiO₃. The device shown in Fig. 5(c) is a long Hall bar, where each segment between voltage probes contains a mesoscale constriction of variable width (0.22–1.35 μm), patterned by e-beam lithography and lift-off of sputtered SiO₂. A 2DEG is accumulated on the exposed SrTiO₃ surface in the Hall bar channel by covering both the device and the adjacent large side gate with an ionic liquid and applying a gate voltage to the side gate.

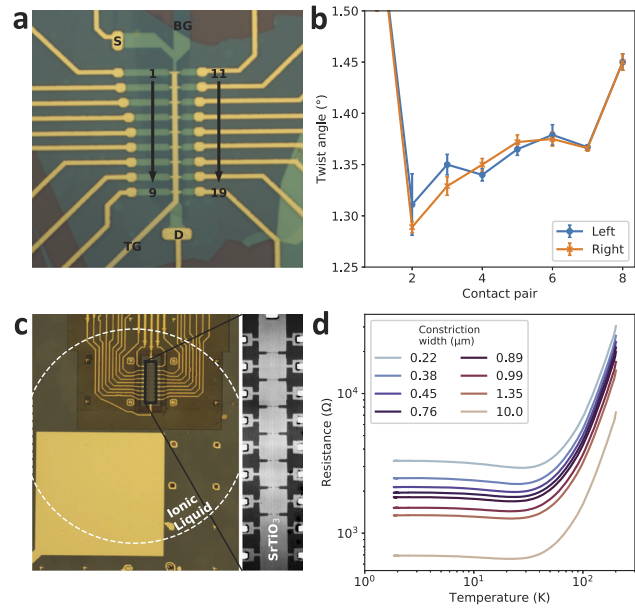


FIG. 5. High throughput measurements on multiterminal devices. (a) and (b) A 22-terminal, twisted bilayer, graphene heterostructure device²⁵ has all contact pairs measured simultaneously, providing information on the local twist angle. Data and figures adapted from Finney *et al.*, Proc. Natl. Acad. Sci. U. S. A. **119**, e2118482119 (2022). Copyright 2022, licensed under a Creative Commons Attribution (CC BY) license. (c) and (d) A 22-terminal SrTiO₃ device²⁶ with fabricated nano constrictions probes temperature-dependent resistance of eight constrictions during a single cooldown.

The lock-in output is used to source an AC current between the top and bottom ends of the Hall bar. The lock-in input channels monitor all 18 voltage probes, measuring 16 voltage differences between adjacent probes (8 voltages on each side of the Hall bar). The measured longitudinal resistance of each segment is shown in Fig. 5(d) as a function of temperature, with all data taken in a single gradual cooldown. Such measurements allow us to study the scaling of charge transport as a function of patterned constriction geometry. We use similar multi-terminal Hall bar devices²⁶ to rapidly assess inhomogeneity in Hall carrier density and mobility, guiding quick iterative adjustments to device fabrication.

In both devices, it would have required a minimum of 16 commercial lock-ins operating in parallel, which is atypical of a transport lab, and prohibitively expensive to acquire for every measurement setup.

NOVEL TRANSPORT DEVICE TOPOLOGIES ENABLED BY FEEDBACK LOCK-IN

The use-case described above shows how the feedback lock-in can be applied directly to existing transport devices to accelerate the measurement process. However, the feedback capability also enables a new type of measurement based on idealized current sources and sinks, which is naturally suited to new device geometries.

The device shown in Fig. 6 is designed to probe the angular flow profile of electrons through a constriction in high-quality, hBN-encapsulated monolayer graphene using seven drain contacts

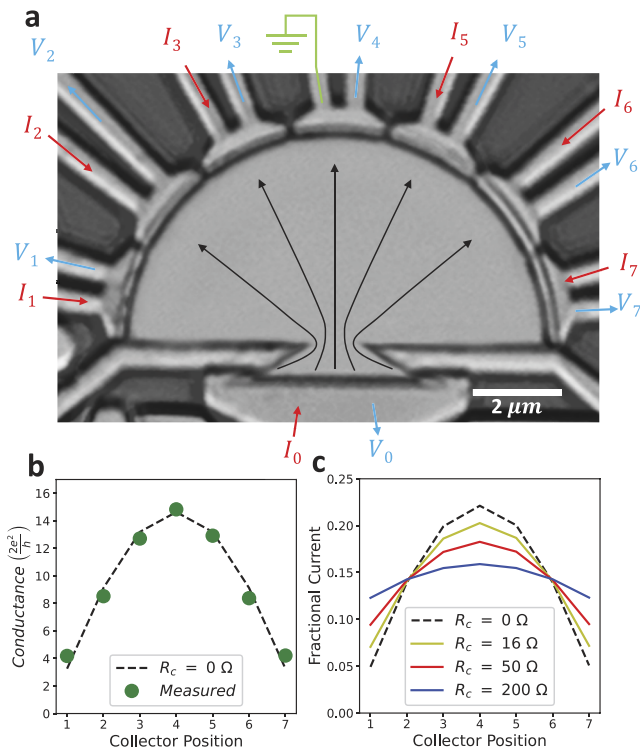


FIG. 6. Transport device enabled by FBL. (a) A $5 \mu\text{m}$ radius, dome-shaped device is designed to measure the angular flow profile of electrons in hBN-encapsulated graphene at cryogenic temperatures. One source and seven drain contacts each have two electrical leads. For each contact, one lead carries current, and the other serves as a voltage probe. The top contact is physically grounded to prevent the whole device from floating; its current is inferred from the remaining other currents. The drain contacts are virtually grounded by ensuring that $(V_n - V_4) = 0$, effectively eliminating the contact resistance (R_c) of the measurement lines and device leads. (b) Measured conductance at 1.4 K as compared to expectations, assuming perfect contacts. The dotted line is based on a single parameter fit of the source constriction's resistance. (c) Theoretical flow profiles based on various drain contact resistances. The trace resistances of the device are $30\text{--}60 \Omega$, and many fridges have filters with resistances $\sim 1 \text{ k}\Omega$, making versions of this measurement based not on feedback, but on transconductance amplifiers, impractical, even if those amplifiers' input offset voltages can be effectively zeroed.

along the perimeter of a semi-circular device-region. If these drains have minimal contact resistance, the angular current distribution through the constriction can be determined by measuring the fractional current that passes through each drain. If the line/contact resistance is not ideal, then voltage differences among the drain contacts can build up and obscure the results, even if low-impedance current preamplifiers are used.

To enable idealized current measurements, we designed our device to have two leads connecting to each ohmic contact on the device. Thus, we are able to monitor the voltage of a given contact, while sourcing the current to the contact via a separate lead. Using these voltage probes, the feedback lock-in can then be used to feed back on the measured voltage of all seven contacts to keep them all at the same potential. We use one of the drains (contact 4) as a ground

reference, and the feedback lock-in maintains a zero-voltage difference between each drain and contact 4. The (nonzero) voltage on the source (V_0) is also referenced to that of contact 4. Conservation of current allows us to determine the current through contact 4 by summing the current through the other leads. Our choice to physically ground one contact rather than use a feedback-driven virtual ground stems from the fact that preamplifier inputs and the back-gate voltage are ground referenced, and it would be intractable to keep the sample voltage within the amplifier bounds, given the high gain and large bias resistances.

We tested the device in a liquid helium 1.4 K cryostat. At our measurement temperature, the mean free path of hBN-encapsulated graphene is known to typically exceed the device dimensions ($10 \mu\text{m}$ diameter semicircle); so, transport should be ballistic. In particular, since we are sourcing current through a constriction, we expect to observe behavior consistent with the Sharvin formula—in other words, the expected angular dependence of current density should be sinusoidal. Measuring at a charge density of $6 \times 10^{11} \text{ cm}^{-2}$ in the graphene, we get a constriction resistance of 196Ω , consistent with an effective constriction width of 750 nm . In Fig. 6(b), we plot the resulting measured conductances as green circles and the theoretical cosine distribution (appropriately discretized) as black dotted lines. The quantitative agreement is striking.

In a typical transport device measurement, there can be ~ 10 to 1000Ω line resistances (depending on whether there are in-line RC filters) and the typical on-chip trace resistance (from wirebond pad to sample region) is $\sim 50 \Omega$, meaning that the best possible line resistance is $\sim 50 \Omega$, with several hundred Ohm being more typical. In Fig. 4(c), we show the theoretical consequences of finite contact/line resistances. These theoretical results are based on ballistic simulations to determine the conductance matrix of the ideal device and then imposing the specified resistances in series with each contact. With even the best-case scenario, it is evident that the finite line resistances will prevent quantitative measurement of the angular distribution. While we do not directly measure the contact resistance in our device, present day graphene/metal contacts^{27,28} can exhibit contact resistivities upward of $35 \Omega\cdot\mu\text{m}$, which would yield a drain contact resistance of 16Ω for leads 1–7. In comparison to this, the line resistances would dominate if not compensated. We plot theoretical current profiles in Fig. 6(c), and interestingly find that the measured profile is closer to ideal than even the 16Ω line. This phenomenology does not necessarily imply that the contact resistances are lower than 16Ω ; however, further studies to determine its origin are beyond the scope of this work.

The near ideal behavior of this device in the ballistic limit demonstrates the technical capability of the feedback lock-in operating in a well-known regime. The more exciting potential for this device and others that rely on virtually grounded contacts is to probe the physics in less-explored regimes, such as the onset of electron hydrodynamics and non-linear transport. We also envision the feedback function to aid in a broader class of mesoscopic systems. For example, it is a challenge to voltage-bias multiple leads in multi-terminal mesoscopic quantum dot devices^{3,29–32} due to unintended voltage offsets. Since our feedback strategy voltage-biases leads in a narrow frequency band around the drive frequency and probes the leads locally, it may readily circumvent this challenge. This could facilitate scattering matrix measurements to probe open quantum

systems. As another example, measurements intended to differentiate between edge and bulk conduction in topological materials³³ can be aided by more effectively shunting edge states.

CONCLUSION

The feedback lock-in is a versatile tool for electrical transport laboratories, both accelerating the pace of discovery by providing parallelizing measurements and enabling new measurement types and geometries. In our implementation, much of the feedback lock-in's capabilities are based on open-source, home-built software, granting experimenters the freedom to add capabilities that are otherwise not available/accessible in commercial lock-in amplifiers. Our implementation is scalable and is ripe for further improvements, with the possibility of greatly enhancing the toolset available to the quantum transport community.

ACKNOWLEDGMENTS

We would like to thank Sawson Taheri for his advice and help with our preamplifier circuit boards and Aaron Sharpe for his useful feedback. Device fabrication, measurements, and analysis were supported by the U.S. Department of Energy, Office of Science, Basic Energy Sciences, Materials Sciences and Engineering Division, under Contract No. DE-AC02-76SF00515. Measurement infrastructure was funded in part by the Gordon and Betty Moore Foundation's EPiQS Initiative through Grant Nos. GBMF3429 and GBMF9460. A.W.B. and E.M. were also supported by the Nano and Quantum Science and Engineering Postdoctoral Fellowship at Stanford University. H.S.H. wishes to acknowledge the Mary Gates Endowment scholarship support for this research/project. D.G.-G. gratefully acknowledges support from the Ross M. Brown Family Foundation. Part of this work was performed at the Stanford Nano Shared Facilities (SNSF), supported by the National Science Foundation, under Award No. ECCS-1542152.

AUTHOR DECLARATIONS

Conflict of Interest

The authors have no conflicts to disclose.

Author Contributions

Arthur W. Barnard: Conceptualization (equal); Software (equal); Supervision (equal); Writing – original draft (equal); Writing – review & editing (equal). **Evgeny Mikheev:** Methodology (equal); Writing – original draft (equal); Writing – review & editing (equal). **Joe Finney:** Methodology (equal); Software (equal); Writing – original draft (equal); Writing – review & editing (equal). **Han S. Hiller:** Investigation (equal); Software (equal); Writing – review & editing (equal). **David Goldhaber-Gordon:** Conceptualization (equal); Funding acquisition (equal); Supervision (equal); Writing – original draft (equal); Writing – review & editing (equal).

DATA AVAILABILITY

The data that support the findings of this study are available from the corresponding author upon reasonable request. Detailed

component designs will be shared with academic researchers upon request. The homebuilt software is available in the following repository: <https://github.com/dgglab/Feedback-Lockin-v2>, Reference number 34.

REFERENCES

- ¹T. J. Thornton, "Mesoscopic devices," *Rep. Prog. Phys.* **58**, 311–364 (1995).
- ²R. Burdett, "Amplitude modulated signals: The lock-in amplifier," in *Handbook of Measuring System Design* (American Cancer Society, 2005).
- ³Z. Iftikhar *et al.*, "Two-channel Kondo effect and renormalization flow with macroscopic quantum charge states," *Nature* **526**, 233–236 (2015).
- ⁴R. K. Kumar *et al.*, "Superballistic flow of viscous electron fluid through graphene constrictions," *Nat. Phys.* **13**, 1182 (2017).
- ⁵N. Nandi *et al.*, "Unconventional magneto-transport in ultrapure PdCoO₂ and PtCoO₂," *npj Quantum Mater.* **3**, 1–6 (2018).
- ⁶M. Serlin *et al.*, "Intrinsic quantized anomalous Hall effect in a moiré heterostructure," *Science* **367**, 900–903 (2020).
- ⁷P. A. Probst and A. Jaquier, "Multiple-channel digital lock-in amplifier with PPM resolution," *Rev. Sci. Instrum.* **65**, 747–750 (1994).
- ⁸G. Gervasoni *et al.*, "A 12-channel dual-lock-in platform for magneto-resistive DNA detection with ppm resolution," in *2014 IEEE Biomedical Circuits and Systems Conference (BioCAS) Proceedings* (IEEE, 2014), pp. 316–319.
- ⁹H. Wi, J. Ko, and J. Chung, "Multi-channel analog lock-in system for real-time motional Stark effect measurements," *Fusion Eng. Des.* **159**, 111664 (2020).
- ¹⁰P. K. Dixon and L. Wu, "Broadband digital lock-in amplifier techniques," *Rev. Sci. Instrum.* **60**, 3329–3336 (1989).
- ¹¹X. Wang, "Sensitive digital lock-in amplifier using a personal computer," *Rev. Sci. Instrum.* **61**, 1999–2001 (1990).
- ¹²D. Uhl, L. Bruder, and F. Stienkemeier, "A flexible and scalable, fully software-based lock-in amplifier for nonlinear spectroscopy," *Rev. Sci. Instrum.* **92**, 083101 (2021).
- ¹³A. Nadgir *et al.*, "SILIA: Software implementation of a multi-channel, multi-frequency lock-in amplifier for spectroscopy and imaging applications," *Meas. Sci. Technol.* **32**, 125501 (2021).
- ¹⁴A. Chighine *et al.*, "An FPGA-based lock-in detection system to enable chemical species tomography using TDLAS," in *2015 IEEE International Conference on Imaging Systems and Techniques (IST)* (IEEE, 2015), pp. 1–5.
- ¹⁵G. Gervasoni, M. Carminati, and G. Ferrari, "Switched ratiometric lock-in amplifier enabling sub-ppm measurements in a wide frequency range," *Rev. Sci. Instrum.* **88**, 104704 (2017).
- ¹⁶G. C. Giaconia, G. Greco, L. Mistretta, and R. Rizzo, "Exploring FPGA-based lock-in techniques for brain monitoring applications," *Electronics* **6**, 18 (2017).
- ¹⁷D. Divakar, K. Mahesh, M. M. Varma, and P. Sen, "FPGA-based lock-in amplifier for measuring the electrical properties of individual cells," in *2018 IEEE 13th Annual International Conference on Nano/Micro Engineered and Molecular Systems (NEMS)* (IEEE, 2018), pp. 1–5.
- ¹⁸G. A. Stimpson, M. S. Skilbeck, R. L. Patel, B. L. Green, and G. W. Morley, "An open-source high-frequency lock-in amplifier," *Rev. Sci. Instrum.* **90**, 094701 (2019).
- ¹⁹C. Zhang, H. Liu, J. Ge, and H. Dong, "FPGA-based digital lock-in amplifier with high-precision automatic frequency tracking," *IEEE Access* **8**, 123114–123122 (2020).
- ²⁰M. Carminati and G. Scandurra, "Impact and trends in embedding field programmable gate arrays and microcontrollers in scientific instrumentation," *Rev. Sci. Instrum.* **92**, 091501 (2021).
- ²¹M. D. Schroer, M. Jung, K. D. Petersson, and J. R. Petta, "Radio frequency charge parity meter," *Phys. Rev. Lett.* **109**, 166804 (2012).
- ²²D. Razmadze *et al.*, "Radio-frequency methods for Majorana-based quantum devices: Fast charge sensing and phase-diagram mapping," *Phys. Rev. Appl.* **11**, 064011 (2019).

- ²³Y. Cao *et al.*, “Unconventional superconductivity in magic-angle graphene superlattices,” *Nature* **556**, 43–50 (2018).
- ²⁴L. Balents, C. R. Dean, D. K. Efetov, and A. F. Young, “Superconductivity and strong correlations in moiré flat bands,” *Nat. Phys.* **16**, 725–733 (2020).
- ²⁵J. Finney *et al.*, “Unusual magnetotransport in twisted bilayer graphene,” *Proc. Natl. Acad. Sci. U. S. A.* **119**, e2118482119 (2022).
- ²⁶E. Mikheev, I. T. Rosen, M. A. Kastner, and D. Goldhaber-Gordon, “Clean ballistic quantum point contact in SrTiO₃,” *arXiv:2110.11535* (2021).
- ²⁷M. Ben Shalom *et al.*, “Quantum oscillations of the critical current and high-field superconducting proximity in ballistic graphene,” *Nat. Phys.* **12**, 318–322 (2016).
- ²⁸C. Kumar *et al.*, “Imaging hydrodynamic electrons flowing without Landauer-Sharvin resistance,” *Nature* **609**, 276–281 (2022).
- ²⁹S. De Franceschi *et al.*, “Out-of-equilibrium Kondo effect in a mesoscopic device,” *Phys. Rev. Lett.* **89**, 156801 (2002).
- ³⁰R. Leturcq *et al.*, “Probing the Kondo density of states in a three-terminal quantum ring,” *Phys. Rev. Lett.* **95**, 126603 (2005).
- ³¹J. Gramich, A. Baumgartner, and C. Schönenberger, “Andreev bound states probed in three-terminal quantum dots,” *Phys. Rev. B* **96**, 195418 (2017).
- ³²W. Pouse *et al.*, “Quantum simulation of an exotic quantum critical point in a two-site charge Kondo circuit,” *arXiv:2108.12691* (2022).
- ³³Z. Fei *et al.*, “Edge conduction in monolayer WTe₂,” *Nat. Phys.* **13**, 677–682 (2017).
- ³⁴Goldhaber-Gordon Group, “Feedback Lockin v2,” <https://github.com/dgglab/Feedback-Lockin-v2> (2022).